

Pressure and electric field dependence of quasicrystalline electronic states in 30° twisted bilayer graphene

Guodong Yu ^{1,2,*}, Mikhail I. Katsnelson,² and Shengjun Yuan ^{1,2,†}

¹Key Laboratory of Artificial Micro- and Nano-structures of Ministry of Education, School of Physics and Technology, Wuhan University, Wuhan 430072, China

²Institute for Molecules and Materials, Radboud University, Heijendaalseweg 135, NL-6525 AJ Nijmegen, Netherlands



(Received 29 March 2020; accepted 25 June 2020; published 9 July 2020)

A 30° twisted bilayer graphene demonstrates the quasicrystalline electronic states with 12-fold symmetry. These states are, however, far away from the Fermi level, which makes conventional Dirac fermion behavior dominating the low-energy spectrum in this system. By using a tight-binding approximation, we study the effect of external pressure and electric field on the quasicrystalline electronic states. Our results show that, by applying the pressure perpendicular to the graphene plane, one can push the quasicrystalline electronic states towards the Fermi level. Then, the electron or hole doping on the order of $\sim 4 \times 10^{14} \text{ cm}^{-2}$ is sufficient for the coincidence of the Fermi level with these quasicrystalline states. Moreover, our paper indicates that applying the electric field perpendicular to the graphene plane can destroy the 12-fold symmetry of these states, and it is easier to reach this in the conduction band than in the valence band. Importantly, the application of the pressure can partially recover the 12-fold symmetry of these states against the electric field. We propose a hybridization picture that can explain all these phenomena.

DOI: [10.1103/PhysRevB.102.045113](https://doi.org/10.1103/PhysRevB.102.045113)

I. INTRODUCTION

The linear band structure of graphene can be modified efficiently by stacking one layer onto another. AA-stacked bilayer graphene shows the band structure of two shifted Dirac cones above and below the Fermi level [1]. The bilayer in AB stacking is characterized (in the simplest approximation) by a band structure with a parabolic touching point [2–6]. Moreover, a twist angle between two layers offers an additional degree of freedom to tune the electronic properties. For example, the slightly twisted bilayer graphene at the magic angle as a model system of strongly correlated electrons has drawn much attention due to the novel electronic properties, such as the flatband [7,8], unconventional superconductivity [9–11], and correlated insulator phases [12]. If the twist angle θ does not satisfy the commensurate condition [13], namely,

$$\cos \theta = \frac{m^2 + 4mn + n^2}{2(m^2 + mn + n^2)}, \quad (1)$$

where m and n are integers, the corresponding bilayer structures will not possess the translational symmetry. Falling into this classification, the 12-fold symmetry and the quasiperiodicity of 30° twisted bilayer graphene has been demonstrated by various measurements, such as the Raman spectroscopy, low-energy electron microscopy/diffraction, transmission electron microscopy, and scanning tunneling microscopy measurements [14–18].

By now, 30° twisted bilayer graphene has been grown successfully on some substrates, such as SiC [15,18], Pt [14], Cu-Ni [16], and Cu [19,20] surfaces. This emergent quasicrystal consisting of two graphene sheets with a perfect crystalline structure has attracted increasing attention because of the coexistence of the quasicrystalline nature and the relativistic properties [14–18,21–24]. Angle-resolved photoemission spectroscopy (ARPES) measurements indicated that the interlayer interaction between the two layers leads to the emergence of the mirror-symmetric Dirac cones inside the Brillouin zone of each graphene layer [14,15,18] and a gap opening at the zone boundary [14]. The critical eigenstates [22,25] and the quantum oscillations with spiral Fermi surfaces [23] were predicted theoretically due to the quasiperiodicity, and the quantum oscillation at low doping concentration was also observed in graphene encapsulated by hexagonal boron nitride [26].

The appearance of the 12-fold symmetric electronic states in 30° twisted bilayer graphene originates from the interaction among the degenerate 12 waves [25]. The 12 waves stand for the Bloch functions at Q_i and \tilde{Q}_i ($i = 0-5$) [see Fig. 1(b)]. Any factor affecting the 12-wave interaction may modify the quasicrystalline electronic states. It has been proved theoretically and experimentally that the external pressure perpendicular to the graphene plane can enhance the interlayer coupling and modify the physical properties of few-layer graphene [11,27–32]. The application of an electric field perpendicular to the graphene plane can break the degeneration of the two layers and affect the quasicrystalline electronic states.

In this paper, our purpose is to study the dependence of the quasicrystalline electronic states on external pressure and the electric field in 30° twisted bilayer graphene. All the pressures

*guodong.yu@whu.edu.cn

†s.yuan@whu.edu.cn

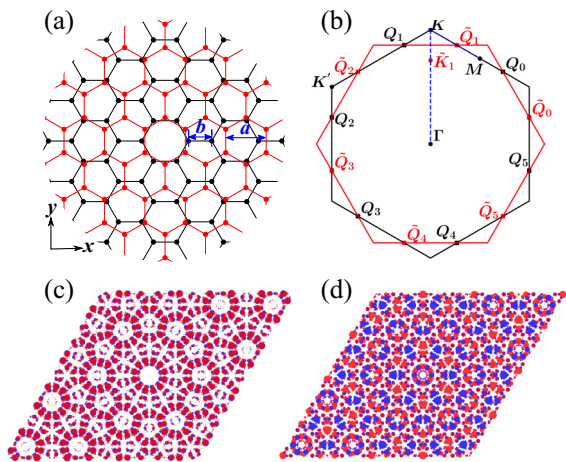


FIG. 1. (a) The structure of 30° twisted bilayer graphene. The periods of the bottom (black) and top (red) layers are a ($= 2.46 \text{ \AA}$) and $3b$ ($= \sqrt{3}a = 4.26 \text{ \AA}$) along the x axis. (b) The Brillouin zones of the two layers. \bar{K}_1 and K are mirror symmetric with respect to the mirror-line Q_1 - \bar{Q}_1 . The Bloch functions of the two layers at Q_i and \bar{Q}_i ($i = 0-5$) are degenerate. (c) and (d) are the charge distributions of the valence-band maximum (VBM) and the conduction-band minimum (CBM) at Q_0 . Blue and red dots correspond to the occupation numbers on the bottom and top layers, respectively. The larger occupation number is denoted by the larger dot.

and the electric fields applied in this paper are perpendicular to the graphene plane. Although the 12-fold symmetric electronic states exist in 30° twisted bilayer graphene, they do not contribute to most of electronic properties because of the long distance from the Fermi level. In this paper, we find the way to tune the energies of these 12-fold symmetric electronic states towards the Fermi level and discuss the stability of the 12-fold symmetries of these states under the external pressure and the electric field.

II. METHODS

The tight-binding model based on the maximally localized Wannier function [33] is adopted to study 30° twisted bilayer graphene under pressure and the electric field. The intralayer hopping energies up to the eighth nearest neighbors are used to describe the graphene monolayer. They are -2.8922 , 0.2425 , -0.2656 , 0.0235 , 0.0524 , -0.0209 , -0.0148 , and -0.0211 eV from the first to the eighth nearest neighbors. The interlayer hopping described by a functional form depends on both distance and orientation. The interlayer hopping function reads

$$t(\mathbf{r}) = V_0(r) + V_3(r)[\cos(3\theta_{12}) + \cos(3\theta_{21})] + V_6(r)[\cos(6\theta_{12}) + \cos(6\theta_{21})]. \quad (2)$$

\mathbf{r} is the projection of the vector connecting two sites on the graphene plane. $r = |\mathbf{r}|$ describes the projected distances between two Wannier functions. θ_{12} and θ_{21} are the angles between the projected interlayer bond and the in-plane nearest-neighbor bonds. They describe the relative orientation of two Wannier functions. The three radial functions depend on ten

TABLE I. The ten interlayer hopping parameters (in units of eV).

y_i	$c_i^{(0)}$	$c_i^{(1)}$	$c_i^{(2)}$
λ_0	0.310	-1.882	7.741
ξ_0	1.750	-1.618	1.848
κ_0	1.990	1.007	2.427
λ_3	-0.068	0.399	-1.739
ξ_3	3.286	-0.914	12.011
x_3	0.500	0.322	0.908
λ_6	-0.008	0.046	-0.183
ξ_6	2.727	-0.721	-4.414
x_6	1.217	0.027	-0.658
κ_6	1.562	-0.371	-0.134

hopping parameters as ($\bar{r} = r/a$),

$$\begin{aligned} V_0(r) &= \lambda_0 e^{-\xi_0 \bar{r}^2} \cos(\kappa_0 \bar{r}), \\ V_3(r) &= \lambda_3 \bar{r}^2 e^{-\xi_3 (\bar{r} - x_3)^2}, \\ V_6(r) &= \lambda_6 e^{-\xi_6 (\bar{r} - x_6)^2} \sin(\kappa_6 \bar{r}). \end{aligned} \quad (3)$$

For twisted bilayer graphene, the relationship between the interlayer distance compression ε and the external pressure P satisfies the Murnaghan equation of state [28],

$$P = A(e^{B\varepsilon} - 1). \quad (4)$$

ε is defined by $1 - h/h_0$, where h and h_0 are the interlayer distances under finite and zero external pressures, respectively. The parameters A and B were determined to be 5.73 GPa and 9.54 from a previous study [27]. The dependence of the ten interlayer hopping parameters on interlayer distance compression is well described by a quadratic fit [27],

$$y_i(\varepsilon) = c_i^{(0)} - c_i^{(1)}\varepsilon + c_i^{(2)}\varepsilon^2, \quad (5)$$

where y_i ($i = 1, \dots, 10$) stands for any one of the ten interlayer hopping parameters. The coefficients $c_i^{(0)}$, $c_i^{(1)}$, and $c_i^{(2)}$ for all interlayer hopping parameters are listed in Table I [27].

It has been shown theoretically that there is no significant atomic reconstruction in free-standing graphene bilayer under a pressure up to 30 GPa [27]. High pressures up to 50 GPa have been applied to suspended graphene bilayer by a diamond-anvil cell experimentally [34]. It turns out that, if water is used as the pressure transmission medium, a pressure with more than 37 GPa is needed to induce a transition from sp^2 to sp^3 bonding between the two layers [34]. But, for the silicone oil pressure transmission medium, the sp^2 - sp^3 transition never occurs even up to 50 GPa [34]. In our paper, we consider pressures up to 30 GPa, which is experimentally reachable and does not change the sp^2 -bonding character in suspended graphene bilayer systems.

The 15/26 approximant [35,36] is used to simulate 30° twisted bilayer graphene. The 15/26 approximant is a periodic moiré pattern obtained by compressing the top layer slightly. The lattice constant of the top layer changes from 2.46 to 2.458 \AA . The two layers share the commensurate period $15 \times \sqrt{3}a = 26 \times \bar{a}$. $\sqrt{3}a$ and \bar{a} are the periods of the bottom and top layers along the x direction, respectively. It has been proved that the 15/26 approximant can reproduce the electronic properties of 30° twisted bilayer graphene accurately

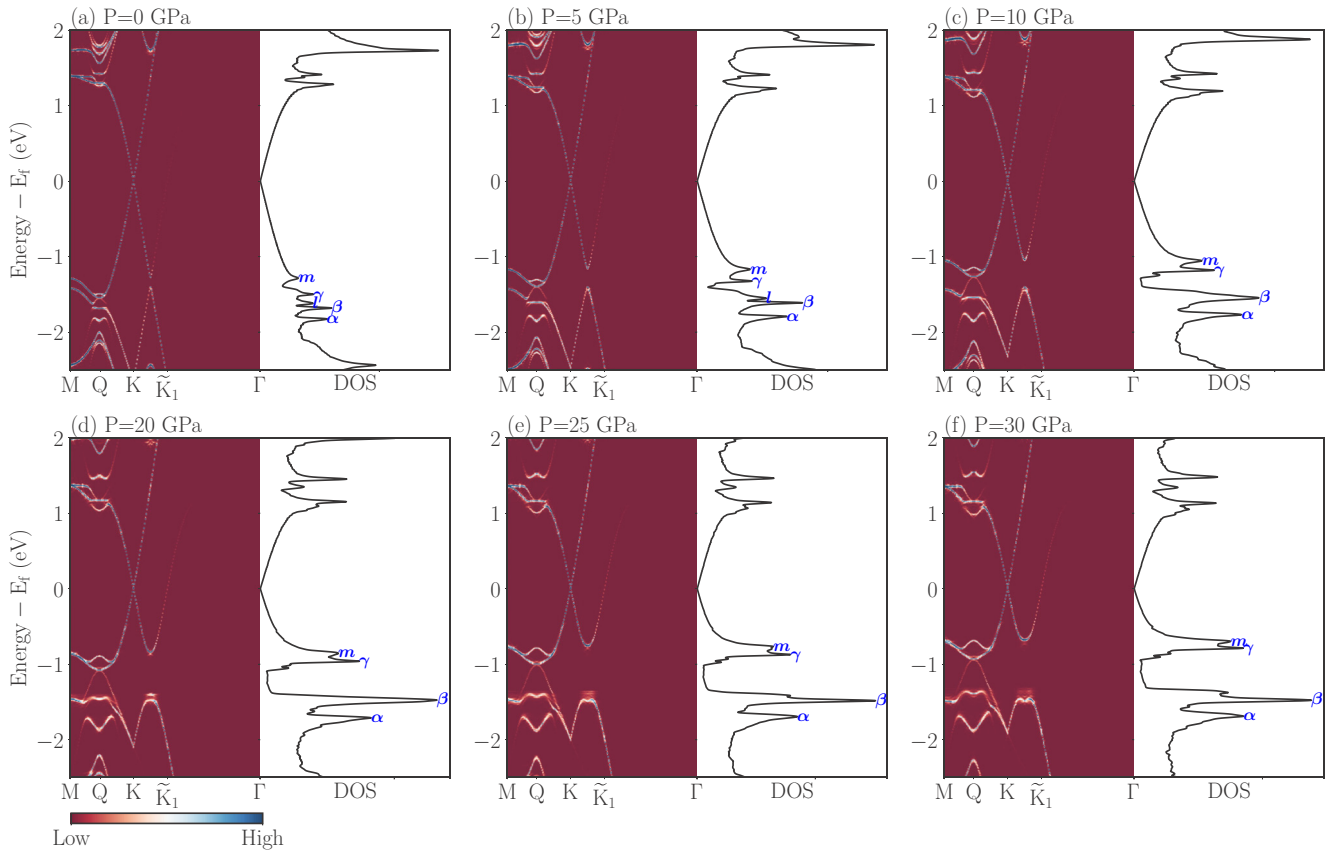


FIG. 2. The comparisons of effective band structures and density of states at several pressures. The k path in the effective band structure is along the dashed blue line shown in Fig. 1(b). The pressure affects the density of states in the valence band stronger than in the conduction band.

[35]. The 12-fold symmetry of the quasicrystalline electronic states can be distinguished within the moiré unit cell [35]. By unfolding the band structure of the 15/26 approximant into the Brillouin zones of the two layers [37,38], one can derive the effective band structure, which can be used to compare with the ARPES measurements.

III. RESULTS AND DISCUSSION

For 30° twisted bilayer graphene, the interlayer interaction causes the appearance of five new van Hove singularities in the density of states in the valence band [25,35]. Three of them, labeled α , β , and γ , are associated with the critical states [25]. It demonstrates the quasicrystalline nature of 30° twisted bilayer graphene. Comparing with the localized states, a critical state still spreads over a large area, so our approximant model cannot reproduce the realistic critical states. Fortunately, the quasicrystalline nature can be recognized by the existence of the 12-fold symmetric states within the moiré unit cell [35], such as the VBM and CBM at Q_0 shown in Figs. 1(c) and 1(d). All the eigenstates at Q_i and \bar{Q}_i ($i = 0-5$) [see Fig. 1(b)] are degenerate and show the same charge distributions. So we use Q to stand for all Q_i and \bar{Q}_i ($i = 0-5$) in the following text. Because we focus on the quasicrystalline electronic states, the VBM and CBM stand for the states at Q in the effective bandstructure.

The density of states and effective band structures under several pressures are shown in Fig. 2. The continuous evolutions of these peaks are given in Fig. 4. As the pressure

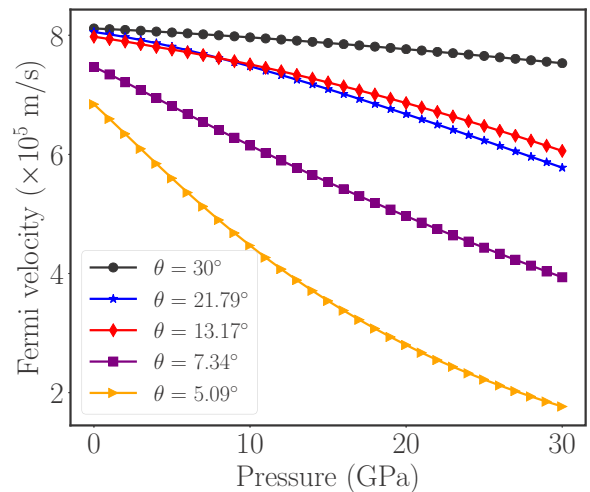


FIG. 3. The change in the Fermi velocity in twisted bilayer graphene with different pressures for several twist angles. The four commensurate twist angles $\theta = 21.79^\circ$, 13.17° , 7.34° , and 5.09° correspond to $(mn) = (1, 2)$, $(2, 3)$, $(4, 5)$, and $(6, 7)$, respectively. The relationship between θ and (m, n) is given in Eq. (1).

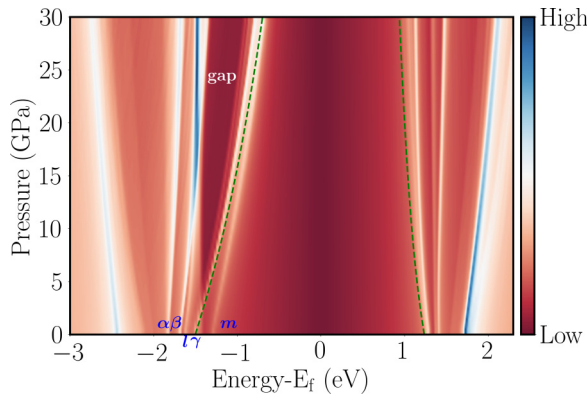


FIG. 4. The density of states under the pressure of less than 30 GPa. Five peaks in the valence band are marked. The positions of the VBM and CBM are shown by the green dashed lines.

increases, the peaks β and m , as well as the peaks γ and l , merge gradually, and a big gap forms between peaks β and γ . The form of the gap is partially attributed to the increasing interaction strength between the Dirac cones at K and \tilde{K}_1 . The Dirac cone at \tilde{K}_1 appears because the Dirac cone at K' is scattered to \tilde{K}_1 [14,39]. The interaction between Dirac cones also reduces the Fermi velocity (shown in Fig. 3). Comparing with some smaller twist angles, the Fermi velocity in 30° twisted bilayer graphene is affected much weaker by pressure. It means the robust Dirac fermion behavior near the Fermi level.

Our results indicate that the 12-fold symmetry of the quasicrystalline electronic states is stable under pressure. The results given in Fig. 4 show that, as the pressure increases from 0 to 30 GPa, the quasicrystalline electronic states move gradually towards the Fermi level and their positions deviate from all peaks of the density of states. So, it becomes easier gradually to tune the Fermi level by electron or hole doping to enhance the contribution of the quasicrystalline electronic states. We will explain this phenomenon below. In Fig. 5, we show the doping concentrations of electrons and holes that are needed for the coincidence of the Fermi level with these quasicrystalline states. For two-dimensional materials,

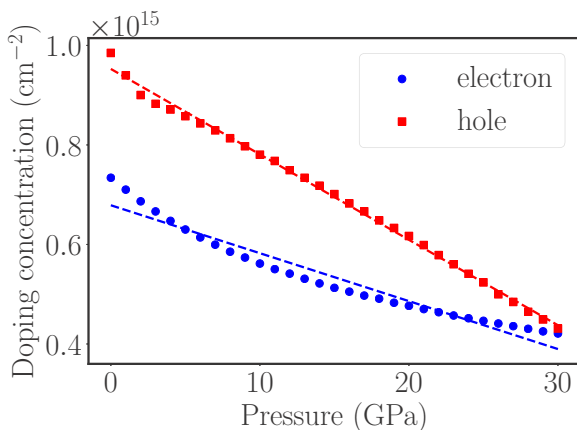


FIG. 5. The concentrations of holes and electrons that are needed to tune the Fermi level to meet the VBM and CBM.

the magnitude of the doping concentration $\sim 10^{14} \text{ cm}^{-2}$ can be realized easily by using ionic liquid gates experimentally [40,41].

Our results show that the quasicrystalline electronic states will lose the 12-fold symmetry if an electric field is applied. We adopt the k -space tight-binding method proposed by Moon *et al.* [25] to understand this phenomenon. In this method, a k_0 -related subspace is spanned by the Bloch functions of the bottom layer at $\mathbf{k} = \mathbf{k}_0 + \tilde{\mathbf{G}}$ and those of the top layer at $\tilde{\mathbf{k}} = \mathbf{k}_0 + \mathbf{G}$. $\tilde{\mathbf{G}}$ (\mathbf{G}) is any reciprocal lattice vector of the bottom (top) layer. In this subspace, the interlayer coupling rule [39] $\mathbf{k} + \mathbf{G} = \tilde{\mathbf{k}} + \tilde{\mathbf{G}}$ is always satisfied. The interlayer matrix element between two layers is written as

$$\begin{aligned} \langle \mathbf{k}, X | H | \tilde{\mathbf{k}}, \tilde{X} \rangle &= \langle \mathbf{k}_0 + \tilde{\mathbf{G}}, X | U | \mathbf{k}_0 + \mathbf{G}, \tilde{X} \rangle \\ &= T(\mathbf{k}_0 + \mathbf{G} + \tilde{\mathbf{G}}) e^{-i\tilde{\mathbf{G}} \cdot \boldsymbol{\tau}_X} e^{i\mathbf{G} \cdot \boldsymbol{\tau}_X}, \end{aligned} \quad (6)$$

where H is the Hamiltonian, U is the interlayer interaction, X (\tilde{X}) is the sublattice A or B (\tilde{A} or \tilde{B}), $\boldsymbol{\tau}_X$ ($\boldsymbol{\tau}_{\tilde{X}}$) is the position of the sublattice in the unit cell, and $T(\mathbf{k}_0 + \mathbf{G} + \tilde{\mathbf{G}})$ is the Fourier component of the interlayer hopping function at $\mathbf{k}_0 + \mathbf{G} + \tilde{\mathbf{G}}$. The notations without and with the tilde signs stand for the quantities belonging to the bottom and top layers, respectively. In the numerical calculation, cutting the k space around \mathbf{k}_0 is needed to construct the Hamiltonian [25]. In this paper, the k -cutoff circle covering the points with $|\tilde{\mathbf{G}}|$ and $|\mathbf{G}| \leq G_0$ is adopted. Here, $G_0 (= \frac{4\pi}{\sqrt{3}a})$ is the length of the smallest reciprocal lattice vector of graphene. This 12-wave approximation, based on the fact that there are 12 k points inside the k -cutoff circle excluding \mathbf{k}_0 , has been proved to be enough to calculate the electronic properties of 30° twisted bilayer graphene [25]. After diagonalizing the Hamiltonian, the $E \sim k_0$ dispersion relation can be derived. We call it a quasiband structure to distinguish the effective band structure obtained by the band unfolding method. It is worth noting that, by comparing the quasiband structure around $\mathbf{k}_0 = \Gamma$ and the effective band structure around Q , the good agreement between them also demonstrates the accuracy of the 12-wave approximation. Enlarging the k -cutoff circle to cover 182 waves [25] will be overcomplete and introduce some redundancy bands. These redundancy bands cannot be detected by ARPES measurements.

At $\mathbf{k}_0 = \Gamma$ and under the 12-wave approximation after folding the k points into the Brillouin zones of the two layers, the subspace shrinks to the collection of the Bloch functions at Q_i ($i = 0-5$) for the bottom layer and those at \tilde{Q}_i ($i = 0-5$) for the top layer [see Fig. 1(b)]. By analyzing the eigenstates of the 12-wave Hamiltonian, a hybridization picture shown in Fig. 6 can be constructed to explain the deviation of the quasicrystalline electronic states from the 12-fold symmetry. The VBM (labeled by $|\delta\rangle$) is the antibonding state after the hybridization between $|\alpha\rangle$ and $|\beta\rangle$, namely,

$$\begin{aligned} |\gamma\rangle &= C_{\gamma\alpha}|\alpha\rangle + C_{\gamma\beta}|\beta\rangle \text{ bonding,} \\ |\delta\rangle &= C_{\delta\alpha}|\alpha\rangle + C_{\delta\beta}|\beta\rangle \text{ antibonding.} \end{aligned} \quad (7)$$

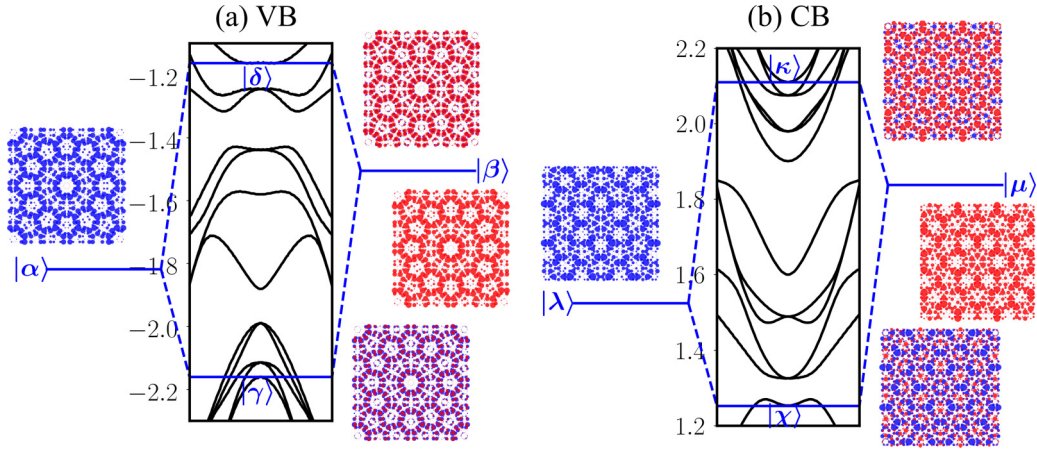


FIG. 6. The quasiband structures around $\mathbf{k}_0 = \Gamma$ and the hybridization pictures for constructing the quasicrystal electronic states in the (a) valence band and the (b) conduction band. The picture shows the example at the 0.1-eV/Å electric field and 5-GPa pressure. It shows clearly that the electric field destroys the 12-fold symmetry of the quasicrystalline electronic states.

$|\alpha\rangle$ and $|\beta\rangle$ are six-wave states of the bottom and top layers, respectively. They can be combined by the Bloch functions as

$$\begin{aligned} |\alpha\rangle &= \frac{1}{\sqrt{6}} \sum_{i=0}^5 (-1)^i |Q_i^-\rangle, \\ |\beta\rangle &= \frac{1}{\sqrt{6}} \sum_{i=0}^5 (-1)^i |\tilde{Q}_i^-\rangle, \end{aligned} \quad (8)$$

where

$$\begin{aligned} |Q_i^-\rangle &= \frac{1}{\sqrt{2}} (|Q_i, A\rangle - |Q_i, B\rangle), \\ |\tilde{Q}_i^-\rangle &= \frac{1}{\sqrt{2}} (|\tilde{Q}_i, \tilde{A}\rangle - |\tilde{Q}_i, \tilde{B}\rangle). \end{aligned} \quad (9)$$

The CBM (labeled $|\chi\rangle$) is the bonding state after the hybridization between $|\lambda\rangle$ and $|\mu\rangle$, namely,

$$\begin{aligned} |\chi\rangle &= C_{\chi\lambda} |\lambda\rangle + C_{\chi\mu} |\mu\rangle \text{ bonding}, \\ |\kappa\rangle &= C_{\kappa\lambda} |\lambda\rangle + C_{\kappa\mu} |\mu\rangle \text{ antibonding}. \end{aligned} \quad (10)$$

$|\lambda\rangle$ and $|\mu\rangle$ are also six-wave states of the two layers. They have the form

$$\begin{aligned} |\lambda\rangle &= \frac{1}{\sqrt{6}} \sum_{i=0}^5 |Q_i^+\rangle \\ |\mu\rangle &= \frac{1}{\sqrt{6}} \sum_{i=0}^5 |\tilde{Q}_i^+\rangle, \end{aligned} \quad (11)$$

where

$$\begin{aligned} |Q_i^+\rangle &= \frac{1}{\sqrt{2}} (|Q_i, A\rangle + |Q_i, B\rangle), \\ |\tilde{Q}_i^+\rangle &= \frac{1}{\sqrt{2}} (|\tilde{Q}_i, \tilde{A}\rangle + |\tilde{Q}_i, \tilde{B}\rangle). \end{aligned} \quad (12)$$

The spatial distributions of the four six-wave states are shown in Fig. 6.

To explain concisely the phenomena about the quasicrystalline electronic states under the pressure and electric field,

we take the VBM as an example. The explanations also apply to the CBM. If there is neither pressure nor electric field, the six-wave states $|\alpha\rangle$ and $|\beta\rangle$ are degenerate. The equivalent hybridization between them, namely, $|C_{\gamma\alpha}|^2 = |C_{\gamma\beta}|^2 = |C_{\delta\alpha}|^2 = |C_{\delta\beta}|^2 = 0.5$ results in the 12-fold symmetric hybridized states $|\gamma\rangle$ and $|\delta\rangle$. A finite pressure will not destroy the degeneracy of $|\alpha\rangle$ and $|\beta\rangle$, and it enhances the hybridization strength. So, applying a finite pressure can push the quasicrystalline electronic state $|\delta\rangle$ up towards the Fermi level. If a finite electric field is applied, the energy splitting between $|\alpha\rangle$ and $|\beta\rangle$ will destroy the 12-fold symmetries of the bonding and antibonding states $|\gamma\rangle$ and $|\delta\rangle$ because of the deviation from the equivalent hybridization. As an example, the hybridization picture for the case of 5-GPa pressure and 0.1-eV/Å electric field is shown in Fig. 6. The bonding and antibonding states show the nonequivalent occupation numbers on the bottom and top layers, namely, the loss of the 12-fold symmetry. For the pressure in the range of 0–30 GPa and the electric field in the range of 0–0.2 eV/Å, the evolutions of the occupation numbers of the VBM and CBM on the bottom layer ($|C_{\delta\alpha}|^2$ and $|C_{\chi\lambda}|^2$) are shown in Fig. 7. Two conclusions

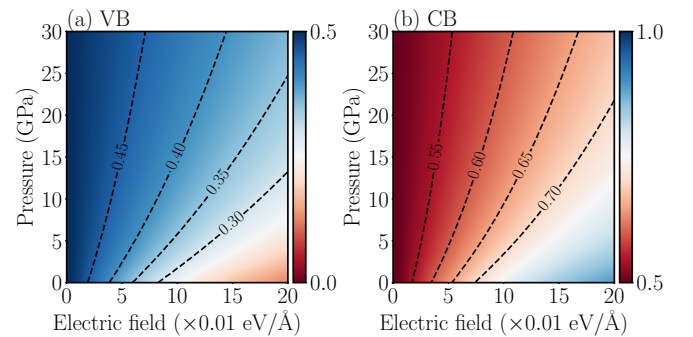


FIG. 7. The evolution of (a) $|C_{\delta\alpha}|^2$ and (b) $|C_{\chi\lambda}|^2$ with the pressure in the range of 0–30 GPa and the electric field in the range of 0–0.2 eV/Å. The counterlines show four conditions where the occupation number on the bottom layer deviates from 0.5 by 0.05, 0.1, 0.15, and 0.2.

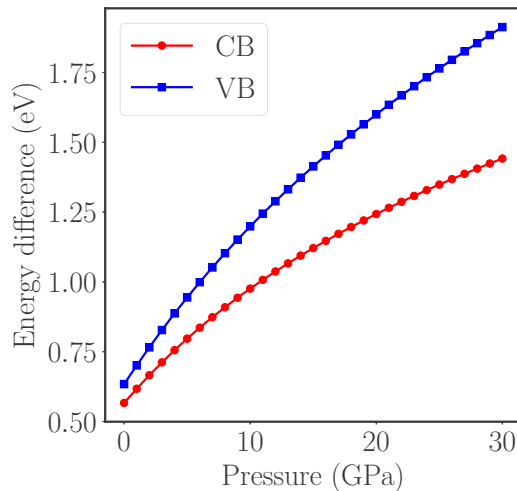


FIG. 8. The energy differences between bonding and antibonding states at a zero electric field for the valence band and the conduction band.

can be drawn from these results. One is that, although the electric field makes the occupation numbers $|C_{\delta\alpha}|^2$ and $|C_{\chi\lambda}|^2$ different from 0.5, the pressure can tune them back closer but not equal to 0.5. It means that the 12-fold symmetry can be partially recovered by applying a finite pressure. The reason behind this is that, for a fixed electric field, a higher pressure can cause shorter interlayer distance and, therefore, smaller on-site energy difference between the two layers. Another conclusion is that the 12-fold symmetry of the CBM is easier to be destroyed than that of the VBM. This is attributed to stronger hybridization strength in the valence band than that of the conduction band (see Fig. 8).

IV. CONCLUSIONS

By using the tight-binding model, we study the dependence of the quasicrystalline electronic states on the external pressure and electric field. We confirm that the pressure can push the energies of these 12-fold symmetric states towards the Fermi level. This phenomenon is attributed to the stronger hybridization between six-wave states of the two layers under higher pressure. Furthermore, the electron or hole doping around $4 \times 10^{14} \text{ cm}^{-2}$ can tune the Fermi level to meet these quasicrystalline electronic states. It can make 30° twisted bilayer graphene manifest the quasicrystalline character in the electronic property. Moreover, the electric field will destroy the 12-fold symmetry of these states. Comparing with the 12-fold symmetric state in the valence band, the 12-fold symmetry of the state in the conduction band is easier to be destroyed. This is because of stronger hybridization in the valence band than that of the conduction band. Importantly, applying external pressure can partially recover the 12-fold symmetry of these states against the electric field by reducing the on-site energy difference between two layers.

ACKNOWLEDGMENTS

This work was supported by the National Natural Science Foundation of China (Grant No. 11774269) and the China Postdoctoral Science Foundation (Grant No. 2018M632902). M.I.K. acknowledges support from the JTC-FLAGERA Project GRANSPORT. Numerical calculations presented in this paper have been partially performed on the supercomputing system in the Supercomputing Center of Wuhan University. Support by the Netherlands National Computing Facilities Foundation (NCF) with funding from the Netherlands Organisation for Scientific Research (NWO) is gratefully acknowledged.

- [1] A. L. Rakhmanov, A. V. Rozhkov, A. O. Sboychakov, and F. Nori, *Phys. Rev. Lett.* **109**, 206801 (2012).
- [2] K. S. Novoselov, E. McCann, S. V. Morozov, V. I. Fal'ko, M. I. Katsnelson, U. Zeitler, D. Jiang, F. Schedin, and A. K. Geim, *Nat. Phys.* **2**, 177 (2006).
- [3] E. McCann and V. I. Fal'ko, *Phys. Rev. Lett.* **96**, 086805 (2006).
- [4] M. Aoki and H. Amawashi, *Solid State Commun.* **142**, 123 (2007).
- [5] S. Latil and L. Henrard, *Phys. Rev. Lett.* **97**, 036803 (2006).
- [6] B. Partoens and F. M. Peeters, *Phys. Rev. B* **74**, 075404 (2006).
- [7] E. Suárez Morell, J. D. Correa, P. Vargas, M. Pacheco, and Z. Barticevic, *Phys. Rev. B* **82**, 121407(R) (2010).
- [8] R. Bistritzer and A. H. MacDonald, *Proc. Natl. Acad. Sci. U.S.A.* **108**, 12233 (2011).
- [9] Y. Cao, V. Fatemi, S. Fang, K. Watanabe, T. Taniguchi, E. Kaxiras, and P. Jarillo-Herrero, *Nature (London)* **556**, 43 (2018).
- [10] H. C. Po, L. Zou, A. Vishwanath, and T. Senthil, *Phys. Rev. X* **8**, 031089 (2018).
- [11] M. Yankowitz, S. Chen, H. Polshyn, Y. Zhang, K. Watanabe, T. Taniguchi, D. Graf, A. F. Young, and C. R. Dean, *Science* **363**, 1059 (2019).
- [12] Y. Cao, V. Fatemi, A. Demir, S. Fang, S. L. Tomarken, J. Y. Luo, J. D. Sanchez-Yamagishi, K. Watanabe, T. Taniguchi, E. Kaxiras, R. C. Ashoori, and P. Jarillo-Herrero, *Nature (London)* **556**, 80 (2018).
- [13] G. Trambly de Laissardière, D. Mayou, and L. Magaud, *Phys. Rev. B* **86**, 125413 (2012).
- [14] W. Yao, E. Wang, C. Bao, Y. Zhang, K. Zhang, K. Bao, C. K. Chan, C. Chen, J. Avila, M. C. Asensio, J. Zhu, and S. Zhou, *Proc. Natl. Acad. Sci. U.S.A.* **115**, 6928 (2018).
- [15] S. J. Ahn, P. Moon, T.-H. Kim, H.-W. Kim, H.-C. Shin, E. H. Kim, H. W. Cha, S.-J. Kahng, P. Kim, M. Koshino, Y.-W. Son, C.-W. Yang, and J. R. Ahn, *Science* **361**, 782 (2018).
- [16] Y. Takesaki, K. Kawahara, H. Hibino, S. Okada, M. Tsuji, and H. Ago, *Chem. Mater.* **28**, 4583 (2016).
- [17] C. Yan, D.-L. Ma, J.-B. Qiao, H.-Y. Zhong, L. Yang, S.-Y. Li, Z.-Q. Fu, Y. Zhang, and L. He, *2D Mater.* **6**, 045041 (2019).
- [18] Y. R. Lin, N. Samiseresht, M. Franke, S. Parhizkar, S. Soubatch, B. Amorim, T. L. Lee, C. Kumpf, F. S. Tautz, and F. C. Bocquet, *arXiv:1809.07958*.
- [19] B. Deng, B. Wang, N. Li, R. Li, Y. Wang, J. Tang, Q. Fu, Z. Tian, P. Gao, J. Xue, and H. Peng, *ACS Nano* **14**, 1656 (2020).

- [20] S. Pezzini, V. Mišeikis, G. Piccinini, S. Forti, S. Pace, R. Engelke, F. Rossella, K. Watanabe, T. Taniguchi, P. Kim, and C. Coletti, *Nano Lett.* **20**, 3313 (2020).
- [21] T. Suzuki, T. Iimori, S. J. Ahn, Y. Zhao, M. Watanabe, J. Xu, M. Fujisawa, T. Kanai, N. Ishii, J. Itatani, K. Suwa, H. Fukidome, S. Tanaka, J. R. Ahn, K. Okazaki, S. Shin, F. Komori, and I. Matsuda, *ACS Nano* **13**, 11981 (2019).
- [22] M. J. Park, H. S. Kim, and S. B. Lee, *Phys. Rev. B* **99**, 245401 (2019).
- [23] S. Spurrier and N. R. Cooper, *Phys. Rev. B* **100**, 081405(R) (2019).
- [24] E. Koren and U. Duerig, *Phys. Rev. B* **93**, 201404(R) (2016).
- [25] P. Moon, M. Koshino, and Y.-W. Son, *Phys. Rev. B* **99**, 165430 (2019).
- [26] N. Leconte and J. Jung, *2D Mater.* **7**, 031005 (2020).
- [27] S. Carr, S. Fang, P. Jarillo-Herrero, and E. Kaxiras, *Phys. Rev. B* **98**, 085144 (2018).
- [28] B. L. Chittari, N. Leconte, S. Javvaji, and J. Jung, *Electron. Struct.* **1**, 015001 (2018).
- [29] B. Padhi and P. W. Phillips, *Phys. Rev. B* **99**, 205141 (2019).
- [30] J. Nicolle, D. Machon, P. Poncharal, O. Pierre-Louis, and A. San-Miguel, *Nano Lett.* **11**, 3564 (2011).
- [31] J. E. Proctor, E. Gregoryanz, K. S. Novoselov, M. Lotya, J. N. Coleman, and M. P. Halsall, *Phys. Rev. B* **80**, 073408 (2009).
- [32] M. Yankowitz, J. Jung, E. Laksono, N. Leconte, B. L. Chittari, K. Watanabe, T. Taniguchi, S. Adam, D. Graf, and C. R. Dean, *Nature (London)* **557**, 404 (2018).
- [33] S. Fang and E. Kaxiras, *Phys. Rev. B* **93**, 235153 (2016).
- [34] Z. Tao, J. Du, Z. Qi, K. Ni, S. Jiang, and Y. Zhu, *Appl. Phys. Lett.* **116**, 133101 (2020).
- [35] G. Yu, Z. Wu, Z. Zhan, M. I. Katsnelson, and S. Yuan, *npj Comput. Mater.* **5**, 122 (2019).
- [36] G. Yu, Z. Wu, Z. Zhan, M. I. Katsnelson, and S. Yuan, *arXiv:1908.08439*.
- [37] H. Nishi, Y.-i. Matsushita, and A. Oshiyama, *Phys. Rev. B* **95**, 085420 (2017).
- [38] P. V. C. Medeiros, S. Stafström, and J. Björk, *Phys. Rev. B* **89**, 041407(R) (2014).
- [39] M. Koshino, *New J. Phys.* **17**, 015014 (2015).
- [40] J. T. Ye, Y. J. Zhang, R. Akashi, M. S. Bahramy, R. Arita, and Y. Iwasa, *Science* **338**, 1193 (2012).
- [41] E. Piatti, D. De Fazio, D. Daghero, S. R. Tamalampudi, D. Yoon, A. C. Ferrari, and R. S. Gonnelli, *Nano Lett.* **18**, 4821 (2018).